Article

An Experimental Study on Static and Dynamic Strain Sensitivity of Smart Concrete Sensors Doped with Carbon Nanotubes for SHM of Large Structures

Andrea Meoni [1], Antonella D'Alessandro [1], Austin Downey [2,3], Enrique García-Macías [4], Marco Rallini [1], A. Luigi Materazzi [1], Luigi Torre[1], Simon Laflamme [3,5], Rafael Castro-Triguero [6] and Filippo Ubertini [1,*]

1 Department of Civil and Environmental Engineering, University of Perugia, Italy; andrea.meoni@unipg.it (A.M.); antonella.dalessandro@unipg.it (A.D.); marco.rallini@unipg.it (M.R.); annibale.materazzi@unipg.it (A.L.M.); luigi.torre@unipg.it (L.T.); filippo.ubertini@unipg.it (F.U.);
2 Department of Mechanical Engineering, Iowa State University, Ames, IA, USA; adowney2@iastate.edu (A.D.);
3 Department of Civil, Construction, and Environmental Engineering, Iowa State University, Ames, IA, USA; adowney2@iastate.edu (A.D.); laflamme@iastate.edu (S.L.);
4 Department of Continuum Mechanics and Structural Analysis, School of Engineering, Universidad de Sevilla, Spain; egarcia28@us.es;
5 Department of Electrical and Computer Engineering, Iowa State University, Ames, IA, USA; laflamme@iastate.edu (S.L.);
6 Department of Mechanics, University of Cordoba, Campus de Rabanales, Cordoba, Spain; me1catrr@uco.es.
* Correspondence: filippo.ubertini@unipg.it; Tel.: +39-075-585-3954

Abstract: The availability of new self-sensing cement-based strain sensors allows the development of dense sensor networks for Structural Health Monitoring (SHM) of reinforced concrete structures. These sensors are fabricated by doping cement-matrix materials with conductive fillers, such as Multi Walled Carbon Nanotubes (MWCNTs), and can be embedded into structural elements made of reinforced concrete prior to casting. The strain sensing principle is based on the multifunctional composites outputting a measurable change in their electrical properties when subjected to a deformation. Previous work by the authors was devoted to material fabrication, modeling and applications in SHM. In this paper, we investigate the behavior of several sensors fabricated with and without aggregates and with different MWCNTs content. The strain sensitivity of the sensors, in terms of fractional change in electrical resistivity for unit strain, as well as their linearity are investigated through experimental testing under both static and dynamically varying compressive loadings. Moreover, the responses of the sensors when subjected to destructive compressive tests are evaluated. Overall, the presented results contribute to improving the scientific knowledge on the behavior of smart concrete sensors and to furthering their understanding for SHM applications.

Keywords: smart concrete sensors, self-sensing materials, structural health monitoring, strain sensitivity, carbon nanotubes, cement-based materials.

1. Introduction

Recent advances in materials and nanotechnologies have enabled the development of multifunctional materials, which have gained popularity in the structural engineering community. In particular, the superior electrical and mechanical properties of nanoengineered powders, such as nanotubes and nanofibers, has resulted in several demonstrations of conductive cementitious materials with excellent sensing capabilities [1,2]. Such materials offer great promise at the monitoring of large-

scale systems, or mesosystems, because they can form large-scale structural components comprising an infinite set of mechanically robust sensors that can be used to measure static and dynamic strain, from which strain-based and vibration-based structural health monitoring (SHM) can be conducted [3,4]. The sensing principle is based on a measurable change in the materials' electrical properties that results from a variation in their geometry. Such materials are often referred to as self-sensing materials [5,6]. However, the technology is yet to be broadly implemented, because of the high cost of the nanoparticles and relatively complex fabrication process related to their dispersion.

Since the '90s, the development of nanoengineered conductive particles represents an important resource for the progress of engineering technologies [7,8]. Examples of application include smart nanocomposites, conductive coatings, nanodevices and nanoengineered materials [9-14]. Among other carbon-based fillers [15,16], carbon nanotubes (CNTs) showed promise for several applications [17-21]. For example, such particles can be used to provide conductive capability to insulating materials, leading to the creation of self-sensing materials [22,23]. Self-sensing materials find great potential in the field of SHM. They can be used to automatically assess the condition of a structural component through the analysis of on-site collected data. This can provide signs of a likely incipient or initial damage, and ultimately lead to condition–based maintenance decisions instead of traditional breakdown- or time-based decisions, resulting in strong economic benefits [24-26]. Self-sensing materials also provide the opportunity to transform a structural component into an infinite or continuous set of sensors, therefore enabling distributed sensing in the form of a dense sensor network [27,28]. This is a powerful advantage over off-the-shelf sensing technologies that are known to have limited scalability due to economic and or technical constraints [29,30]. The self-sensing ability of cement-based materials or sensors is obtained through mapping variations in strain to variations in electrical characteristics of the material such as electrical resistivity or conductivity [31-39]. Literature demonstrates that suitable fillers for cementitious matrices yielding self-sensing materials are carbon-based particles of short, micro or nano sizes [40-43]. Among available powders, carbon nanotubes have excellent electrical properties and have morphological characteristics suitable to produce conductive network in composite materials such as concrete [44-47]. Their high specific surface and their nanometric size enhance their electrical performance. Literature shows a growing interest in such nanofillers [48-52]. Research has studied dispersion strategies in different types of matrices [53,5454] and fabrication processes [54-56], and conducted experimental investigations mainly focused on quasi-static loads [57-62]. The dispersion of CNTs is an intricate task due to the presence of Van der Waals forces among the single tubes which lead to the formation of bundles [63,64]. Currently available dispersion methods in aqueous solutions (i.e., cementitious materials during the mixing stage) include chemical, physical and mechanical methods. A good dispersion is essential to achieve homogeneous and repeatable properties of the material. In addition, different quantities of nanoparticles influence chemical, physical and mechanical properties. The use of self-sensing cementitious materials for vibration-based monitoring was previously investigated by the authors, with particular attention to fabrication processes and electromechanical modelling of dynamic behaviors [65,66]. Research has demonstrated the potential of self-sensing cementitious materials at vibration-based SHM, but concluded that further studies are needed to better investigate signal quality and sensors' response characteristics with varying amount of nanotubes and with or without aggregates.

This paper presents an experimental study on the behavior of a set of cement-based strain sensors fabricated with and without aggregates and with different MWCNT contents. The investigation covers strain sensitivity and linearity of the sensors under both static and dynamic varying compressive loadings. A study on the response of the sensors subjected to destructive tests carried out using a displacement controlled compression load completes the work. Overall, the presented results extend those obtained in previous research [54] regarding the effect of aggregates and different filler contents on the sensors' behavior.

The paper is organized as follows. Section 2 describes the material properties and the preparation process of the samples. Also, the experimental methodology and the laboratory configuration for the

electrical, electromechanical and destructive tests are illustrated. Section 3 presents the experimental results. Section 4 concludes the paper with a discussion of the obtained results.

2. Materials and Methods

2.1. Materials and preparation process of samples

The cementitious sensors under investigation are fabricated with and without aggregates (cement paste and concrete matrices). The water/cement ratio was taken as 0.45 for all the admixtures. The cement was type 42.5, Pozzolanic. The mean diameter of sand particles was lower than 4 mm, while the mean diameter of medium gravel particles was between 4 and 8 mm. For neat concrete and nanofilled materials, a second-generation superplasticizer based on polycarboxylate ether polymers was introduced in a variable amount in order to obtain similar workability for all the admixtures. Tables 1 and 2 list the different mix designs of cement pastes and concretes without filler (Table 1) and with different contents of MWCNTs (Table 2). The quantities refer to one cubic meter of produced material. In Table 2, ΔV_P, ΔV_M and ΔV_C represent the incremental volume with respect to the reference cubic meter, composed of nanotubes and surfactant for composite cement paste and concrete, respectively, $n_{\%}$ is the percentage of added filler with respect to the mass of the cement, and C_p, C_m and C_c are the particular cement contents in the mixes of cement paste and concrete, respectively. The filler contents ranged from 0 to 1%, with step increments of 0.25%, and 1.5% for all specimens.

The carbon nano-fillers were MWCNTs, Arkema Graphistrength C100 [67]. They appear as black powder, with carbon content greater than 90% in weight, and an apparent density of 50 – 150 kg/m^3. The mean number of walls is between 5 and 15, with an outer mean diameter of 10 – 15 nm and a length of 0.1 – 10 μm. The surface area of the MWCNTs is approximately 100-250 m^2/g. Their elastic modulus is greater than 1 TPa and their tensile strength around 150 GPa.

Figure 1 describes the preparation procedure for the fabrication of paste and concrete cubes with MWCNTs. The process is divided into two subsequent steps. First the carbon nanotubes were dispersed into water with a physical surfactant (i), mechanically mixed (ii) and sonicated (iii). Second, the suspension was added to cement, fine and coarse aggregates to achieve cement paste and concrete, respectively (iv). A plasticizer was added to obtain similar workability of the fresh mixtures. The materials were casted into oiled molds and the electrodes were embedded to a depth of about 40-45 mm (v). After 48 hours, the samples were unmolded and cured for 28 days at laboratory conditions (vi). The fabricated samples are cubes of 5 cm sides.

Table 1. Mix design of cement paste and concrete without carbon fillers relative to one cubic meter of self-sensing materials.

Components	Cement Paste [kg/m^3]	Concrete [kg/m^3]
Cement 42.5 Pozzolanic	1277	524
Water	574	234
Surfactant	-	-
Sand (0 - 4 mm)	-	951
Medium Gravel (4 – 8 mm)	-	638
Superplasticizer	-	2.62
Water/Cement Ratio	0.45	0.45

Table 2. Mix design of cement paste and concrete with carbon fillers relative to one cubic meter of self-sensing materials.

Components	Cement Paste [kg/m^3]	Concrete [kg/m^3]

Preprints (www.preprints.org) | NOT PEER-REVIEWED | Posted: 7 February 2018 doi:10.20944/preprints201802.0063.v1

Peer-reviewed version available at Sensors 2018, 18, 831; doi:10.3390/s18030831

Cement 42.5 Pozzolanic	$C_p = 1277 \cdot \frac{1\text{m}^3}{1\text{m}^3 + \Delta V_{PA}}$	$C_c = 524 \cdot \frac{1\text{m}^3}{1\text{m}^3 + \Delta V_{CO}}$
Water	$0.45 \cdot C_p$	$0.45 \cdot C_c$
MWCNTs	$n_{\%} \cdot C_p$	$n_{\%} \cdot C_c$
Surfactant	$n_{\%} \cdot C_p$	$n_{\%} \cdot C_c$
Sand (0 - 4 mm)	-	$1.8 \cdot C_c$
Medium Gravel (4 – 8 mm)	-	$1.22 \cdot C_c$
Superplasticizer	variable	variable
Water/Cement Ratio	0.45	0.45

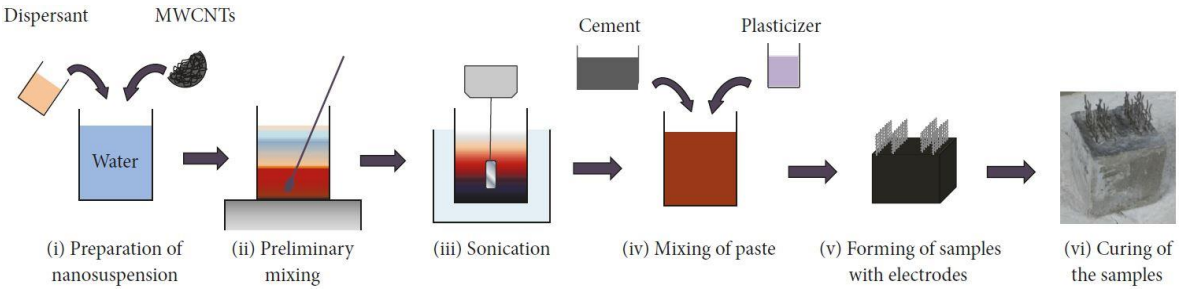

Figure 1. Preparation procedure of paste and concrete samples with carbon nanotubes.

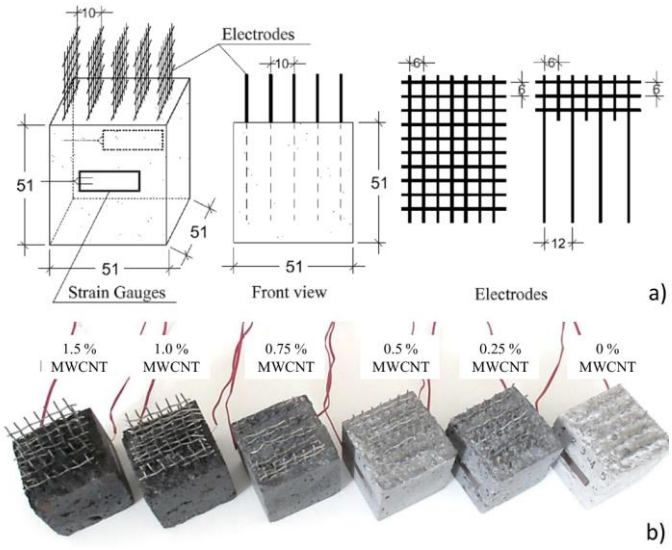

Figure 2. (**a**) Geometry of specimens and electrodes (dimensions are in mm); (**b**) Picture of samples with 1.5, 1.0, 0.75, 0.5, 0.25 and 0% (from left to right) MWCNTs.

Each cube is equipped with five embedded mesh stainless steel electrodes placed at a mutual distance of 10 mm. They are instrumented with two 20 mm long strain gauges installed on opposite sides. Figure 2a shows the geometry of the samples, the position of the electrodes and strain gauges, and the dimensions of a single electrode. For concrete specimens, the wire mesh was modified to be embedded at a distance of 12 mm (Figure 2a) not to interfere with coarse aggregates. The applied loads during the electromechanical tests were uniaxial, perpendicular to the electrodes. The strain gauges were positioned at the center of the samples' surfaces along the loading direction to measure the applied strain. The presence of different levels of MWCNTs resulted in different visual appearance for the samples. Figure 2b is a picture of samples with 1.5, 1.0, 0.75, 0.5, 0.25 and 0% MWCNTs contents.

2.2. Electrical tests

Electrical tests were conducted using DC current with a 4-probe method. A stabilized current was applied at two electrodes at a mutual distance of 30 mm, and the voltage, $V(t)$, between the two adjacent electrodes, which are at a mutual distance of 10 mm, was measured for each sample. The data acquisition system used for acquiring measurements and providing the stabilized current was a NI PXIe-1073 device equipped with a high speed digital multimeter, model NI PXI-4071 and a current generator, model NI PXI-4130, capable of providing a four-quadrant ±20 V and ±2 A output on a single isolated channel. The electrical resistance of the specimens, evaluated after 6000 s of constantly applied current to achieve a stable level of polarization in the material, was obtained using Ohm's law:

$$R_t = \frac{V(t)_{t=t_p}}{I}, \quad (1)$$

where I is the applied constant current, $V(t)$ is the measured variations of voltage over time, and t_p is the polarization time. The electrical conductivity, σ, was computed as follows:

$$\sigma = \left(R_{t=t_p} \cdot \frac{A}{d} \right)^{-1} = \left(\frac{V_{t=t_p}}{I} \cdot \frac{A}{d} \right)^{-1}, \quad (2)$$

where R is the electrical resistance, A is the value of the section area of the sample, d is the distance between the electrodes.

2.3. Electromechanical tests

The electromechanical tests for the assessment of the self-sensing capabilities were conducted using a servo-controlled pneumatic universal testing machine, model IPC Global UTM14P, with 196 kN of load capacity. The sensors were subjected to two different loading histories: the first one consisted of loading-unloading cycles between 0.5 and 2 kN at a constant low speed (Figure 3a), while the second one consisted of a dynamic load with amplitude varying between 0.5 and 1.5 kN at increasing frequencies, from 0.25 Hz to 0.5, 1, 2, 4, and 6 Hz (Figure 3b). Average compressive strain of the specimens was obtained by the two resistive strain gauges applied onto opposite faces, while the voltage variations over time were recorded through the data acquisition system. Similarly to the electrical characterization tests, the 4-probe method was used for this test. The data acquisition system was a NI PXIe-1073, instrumented with a high speed digital multimeter, NI PXI-4071, a source measure unit, model NI PXI-4130, providing a stabilized voltage or current on a single isolated channel, and a data acquisition card, NI PXIe-4330, for strain gauge measurements.

The electrical sensitivity derives from several effects: the intrinsic resistance of carbon nanofillers and the cementitious matrix, the contact conduction among the nanotubes, and the tunneling and field emission conductions due to nanosize dimensions of the nanotubes [29,61,64]. The relationship between the variation of electrical resistance, ΔR, and the axial strain, ε, can be assumed as follows (similar to the electrical strain gauges):

$$\Delta R / R_0 = -GF \cdot \varepsilon, \quad (3)$$

where R_0 is the electrical resistance without load and GF is the gauge factor of the material.

Preprints (www.preprints.org) | NOT PEER-REVIEWED | Posted: 7 February 2018 doi:10.20944/preprints201802.0063.v1

Peer-reviewed version available at Sensors 2018, 18, 831; doi:10.3390/s18030831

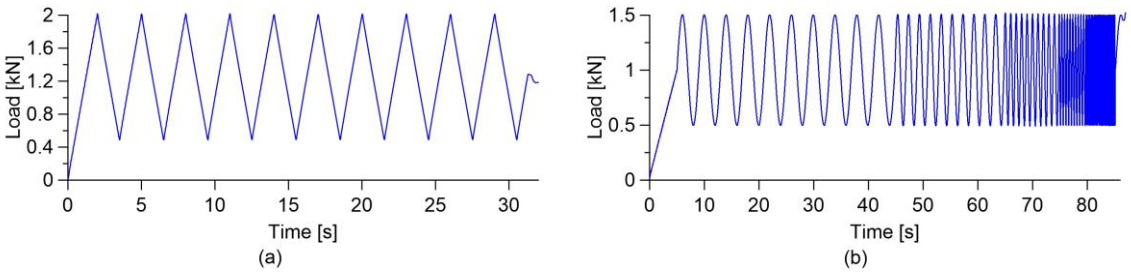

Figure 3. (**a**) Cyclical uniaxial load; (**b**) Dynamic uniaxial load.

2.4. Destructive tests

Destructive compression tests were performed by applying a uniaxial compression load under displacement control to the nanocomposite cement-based sensors using an electric-servo test machine, model Advantest 50-C7600 by Controls, equipped with a servo-hydraulic control unit model 50-C 9842. The axial displacement, applied with a constant speed of 2.0 μm/s, was measured through three linear variable differential transformers (LVDTs) connected to the test machine. The average displacement, *h*, was considered to obtain the axial strain, ε, following the equation:

$$\varepsilon = \frac{l'-l}{l} = \frac{(l-h)-l}{l}, \quad (4)$$

where l is the original length and l' is the final length of the specimen. Applied stress on the sample, σ_F, was calculated as follows:

$$\sigma_F = F / A, \quad (5)$$

where F is the applied load measured through the load cell of the machine and A is cross-section of the sample.

During the application of the compression load and up to failure of the specimens, electrical measurements were carried out with a 4-probe method using a high speed digital multimeter, model NI PXI-4071, and a DC current generator, model NI PXI-4130, both hosted into a chassis, model NI PXIe-1073, as illustrated in the case of electrical tests. This allows to test the sensing function within the whole range of deformation of the material.

3. Results

3.1 Percolation threshold

Figure 4 plots of the calculated electrical conductivity for paste and concrete specimens according to Equation (2). Results show that the percolation threshold is identifiable at 1% of MWCNTs content for paste specimens, and between 1% and 1.5% of MWCNTs content for composite concrete. The paste specimen with 1.5% weight content of nanotubes with respect to the weight of cement exhibits a reduction in electrical conductivity compared to the one with 1.0% MWCNTs content. This can be attributed to a less homogeneous MWCNTs dispersion because this specimen is the one containing the largest amount of nanotubes among those investigated. Another observation on the results is that paste samples without nanotubes are more conductive than plain concrete specimens, while after percolation the two materials reach approximately the same conductivity. It follows that the addition of nanotubes has less effects on the variation of electrical conductivity in the case of cement paste compared to the case of concrete. In addition, the presence of aggregates in the concrete mixes results in a smaller

effective volume to be filled by the MWCNTs particles, therefore making conductive chains more difficult to form in a cement and sand matrix relative to a cement-only matrix [63].

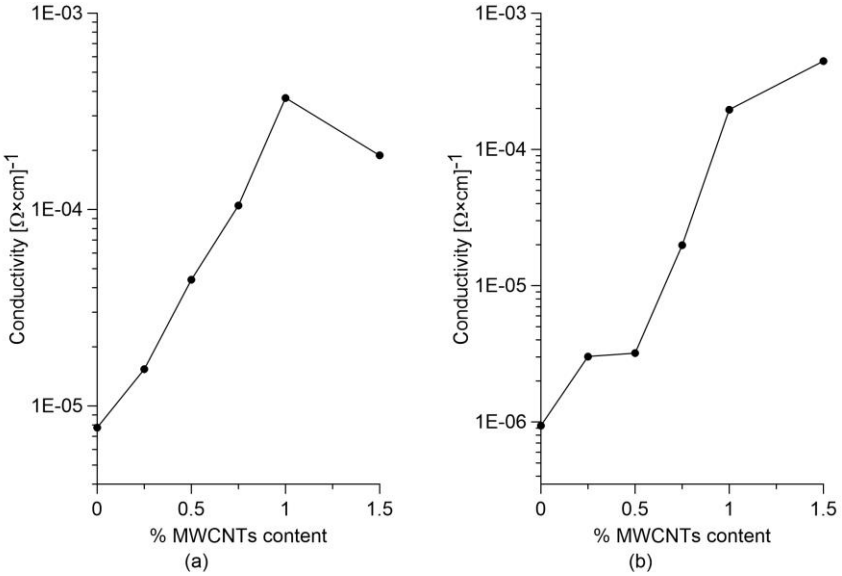

Figure 4. Electrical conductivity variation for different MWCNTs content in **(a)** paste samples; and (**b**) concrete samples.

3.2 Linearity of the sensors under cyclic compression loads

The strain sensing capability of the different specimens and their linearity are investigated through compressive tests with cyclic loads. The plots in Figures 5 and 6 report the relative change in electrical resistance versus the applied strain of nanocomposite paste and concrete samples, respectively. In both cases, the base materials without nanotubes exhibit clear strain sensitivity that is however characterized by a significant non-linear relationship between the relative change in electrical resistivity and the applied deformation (Figure 5a, 6a). This phenomenon is more evident in the concrete sample where the response of the base material also exhibits a hysteresis (Figure 6a). The addition of carbon nanotubes to the base materials regularizes such strain-sensing response, making it more linear and reversible, up to a volume fraction of carbon nanotubes that is slightly below the percolation threshold (Figure 5b, 5c, 5d, 6b, 6c, 6d). At percolation, the response becomes slightly non-linear for both materials (Figure 5e, 6e), while the linearity seems to recover for higher nanotube content (Figure 5f, 6f).

3.3 Strain sensitivity and signal quality

Figure 7 shows values of the gauge factor, *GF*, computed from the electromechanical tests depicted in Figures 5 and 6, highlighting in particular the effect of a varying content of MWCNTs. As already observed above, both cement-paste and concrete specimens have demonstrated a clear strain-sensing capability though non-linear in nature, corresponding to relatively high *GF* values. Increasing the content of MWCNTs changes the conductive mechanisms and, therefore, the values of *GF*. Relatively large values of *GF* are obtained at 0.5 % of MWCNTs contents for cement paste and 1.0 % of MWCNTs for concrete specimens, respectively. Cement paste specimen with 1.5% of MWCNTs seems to be an outlier which could be associated to a less homogeneous MWCNTs dispersion, as already commented when introducing the percolation curves. These optimal amounts of MWCNTs resulting into the largest values of *GF* are close to the identified percolation thresholds, as also discussed in other literature works [57], confirming that the specimens exhibit an enhanced piezoresistive behavior near the percolation threshold. When the MWCNTs content exceeds this optimal quantity, the nanotubes create a continuous network, and consequently an applied strain does not significantly modify the interactions

Preprints (www.preprints.org) | NOT PEER-REVIEWED | Posted: 7 February 2018 doi:10.20944/preprints201802.0063.v1

Peer-reviewed version available at Sensors 2018, 18, 831; doi:10.3390/s18030831

between nanotubes that are already in contact. On the other hand, when MWCNTs content is lower than the optimal value, a reduction in *GF* is observed because the average distance between nanotubes is too big to allow transfer of electrons from one nanotube to the other.

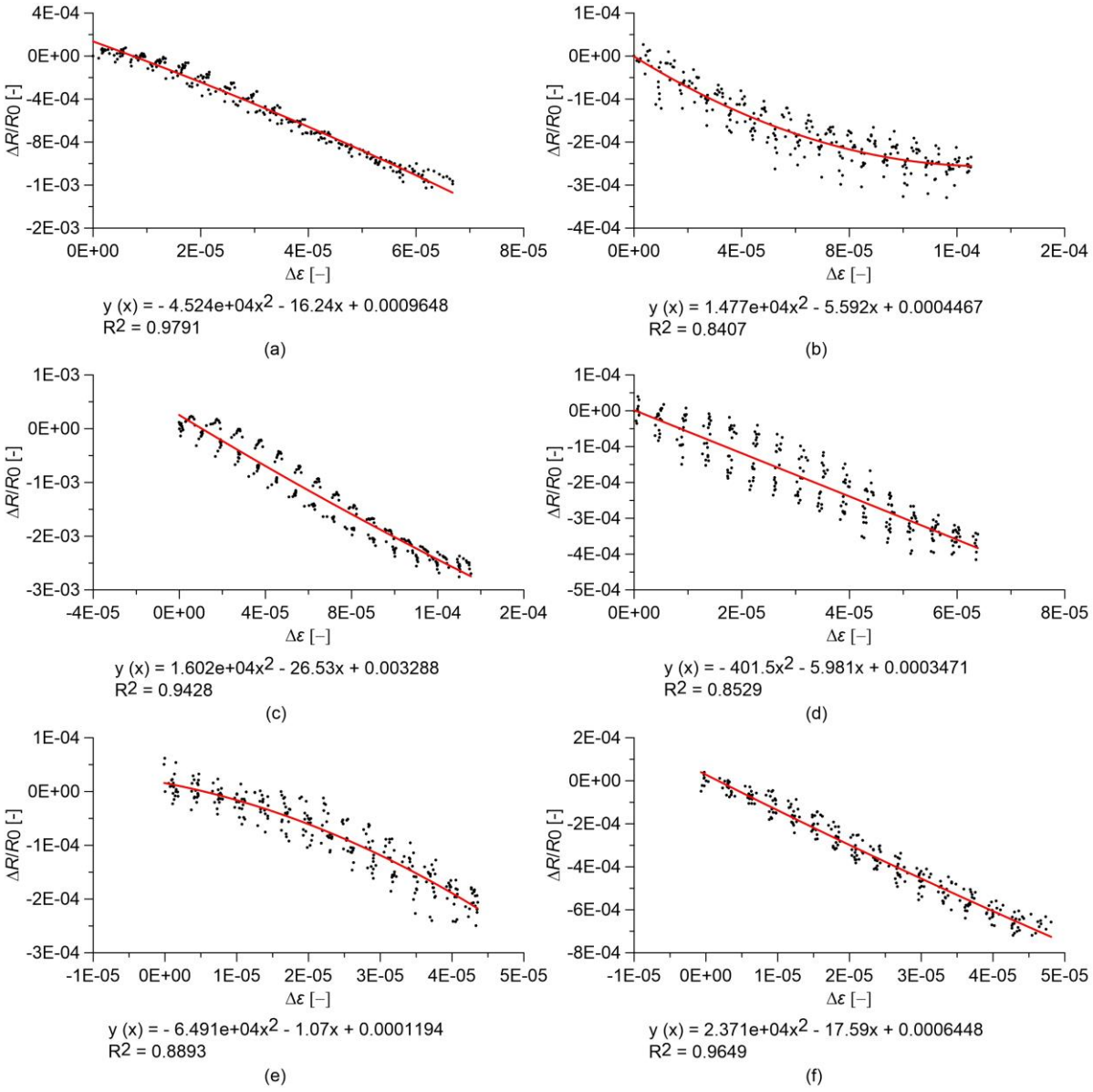

Figure 5. Relative change in electrical resistance versus applied strain of nanocomposite cement paste specimens under cyclic compression loads. In the plots, R_0 is the electrical resistance value with a preload of 0.5 kN and equations of quadratic regression lines are reported: (**a**) Paste with 0.00% of MWCNTs; (**b**) Paste with 0.25% of MWCNTs; (**c**) Paste with 0.50% of MWCNTs; (**d**) Paste with 0.75% of MWCNTs; (**e**) Paste with 1.00% of MWCNTs; (**f**) Paste with 1.50% of MWCNTs.

Preprints (www.preprints.org) | NOT PEER-REVIEWED | Posted: 7 February 2018 doi:10.20944/preprints201802.0063.v1

Peer-reviewed version available at Sensors 2018, 18, 831; doi:10.3390/s18030831

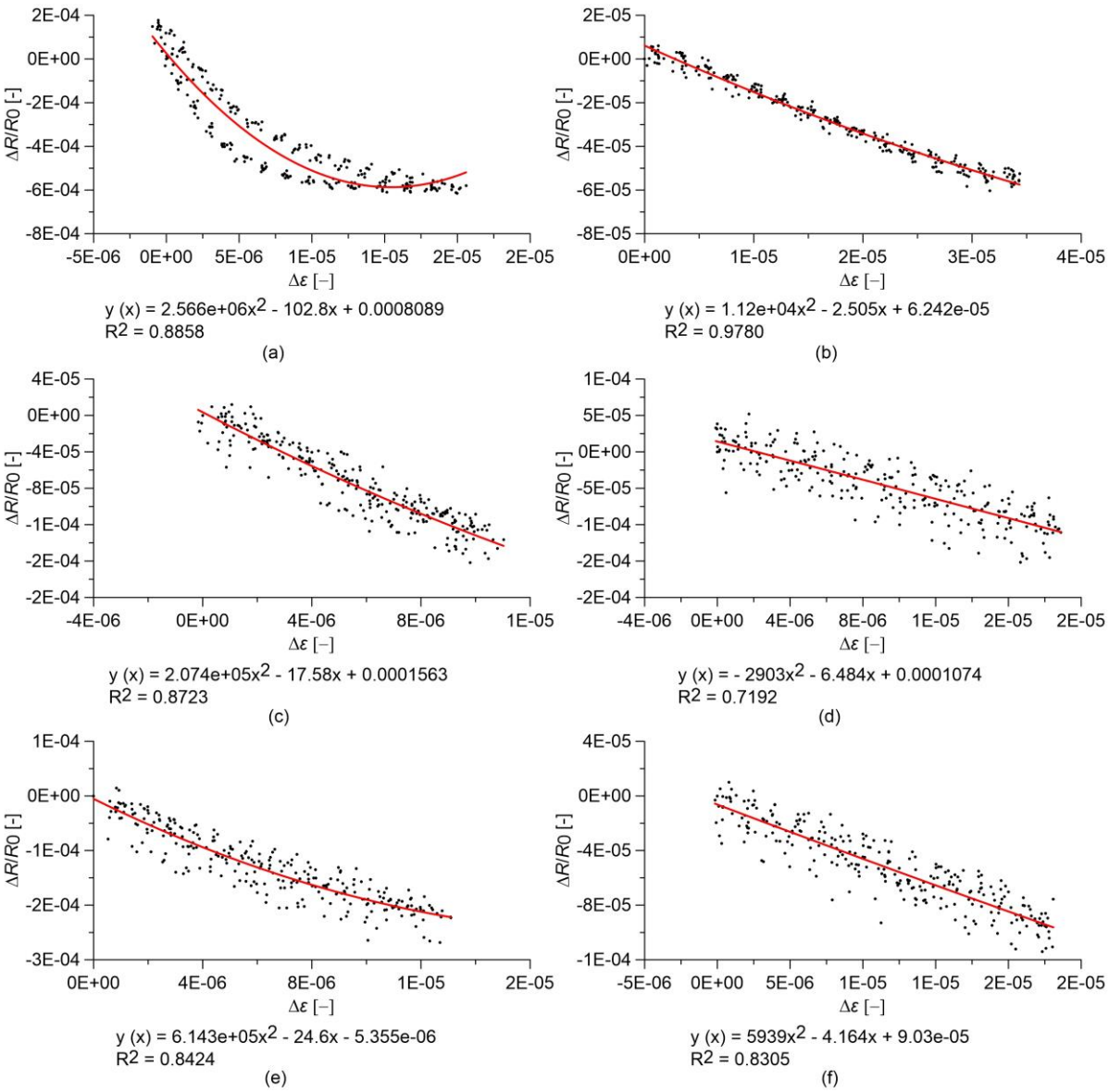

Figure 6. Relative change in electrical resistance versus applied strain of nanocomposite concrete specimens under cyclic compression loads. In the plots, R_0 is the electrical resistance value with a preload of 0.5 kN and equations of quadratic regression lines are reported: (**a**) Concrete with 0.00% of MWCNTs; (**b**) Concrete with 0.25% of MWCNTs; (**c**) Concrete with 0.50% of MWCNTs; (**d**) Concrete with 0.75% of MWCNTs; (**e**) Concrete with 1.00% of MWCNTs; (**f**) Concrete with 1.50% of MWCNTs.

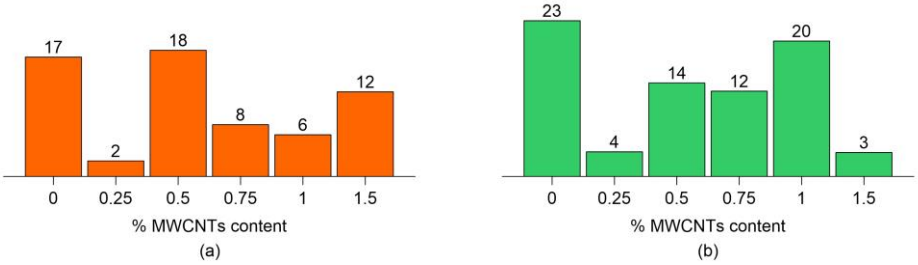

Figure 7. Gauge factor as a function of MWCNTs content for **(a)** paste samples; and (**b**) concrete samples.

Preprints (www.preprints.org) | NOT PEER-REVIEWED | Posted: 7 February 2018 doi:10.20944/preprints201802.0063.v1

Peer-reviewed version available at Sensors 2018, 18, 831; doi:10.3390/s18030831

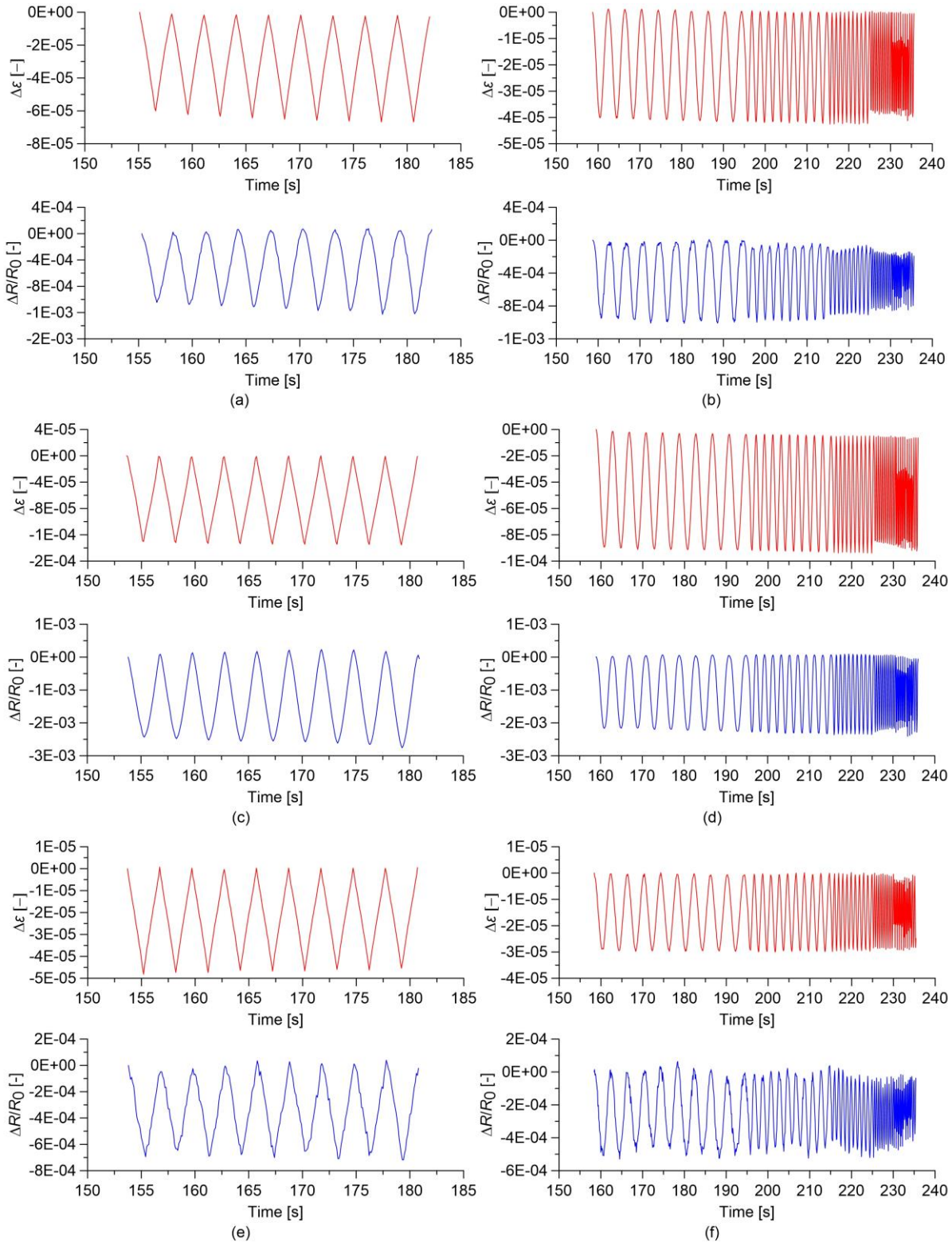

Figure 8. Time histories of the relative change in electrical resistance, $\Delta R/R_0$, and of the applied strain, $\Delta\varepsilon$, obtained from the electromechanical tests. In the plots, R_0 is the electrical resistance value with a preload of 0.5 kN: (**a**) Cyclic load applied on paste with 0.00% of MWCNTs; (**b**) Dynamic load applied on paste with 0.00% of MWCNTs; (**c**) Cyclical load applied on paste with 0.50% of MWCNTs; (**d**) Dynamic load applied on paste with 0.50% of MWCTs; (**e**) Cyclical load applied on paste with 1.50% of MWCNTs; (**f**) Dynamic load applied on paste with 1.50% of MWCNTs.

Preprints (www.preprints.org) | NOT PEER-REVIEWED | Posted: 7 February 2018 doi:10.20944/preprints201802.0063.v1

Peer-reviewed version available at Sensors 2018, 18, 831; doi:10.3390/s18030831

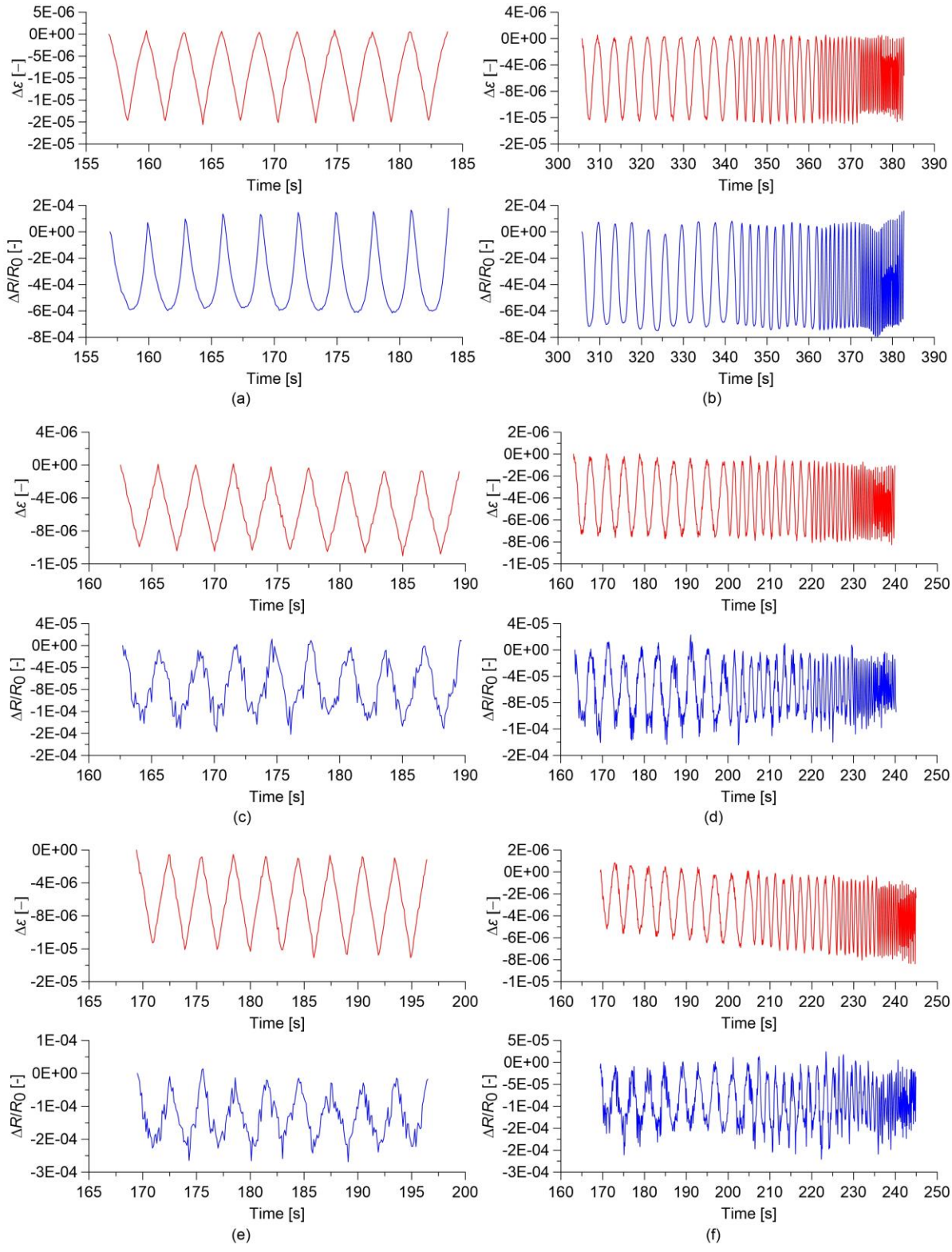

Figure 9. Time histories of the relative change in electrical resistance, $\Delta R/R_0$, and of the applied strain, $\Delta\varepsilon$, obtained from the electromechanical tests. In the plots, R_0 is the electrical resistance value with a preload of 0.5 kN: (**a**) Cyclic load applied on concrete with 0.00% of MWCTs; (**b**) Dynamic load applied on concrete with 0.00% of MWCNTs; (**c**) Cyclic load applied on concrete with 0.50% of MWCNTs; (**d**) Dynamic load applied on concrete with 0.50% of MWCNTs; (**e**) Cyclic load applied on concrete with 1.00% of MWCNTs; (**f**) Dynamic load applied on concrete with 1.00% of MWCNTs.

Preprints (www.preprints.org) | NOT PEER-REVIEWED | Posted: 7 February 2018 doi:10.20944/preprints201802.0063.v1

Peer-reviewed version available at Sensors 2018, 18, 831; doi:10.3390/s18030831

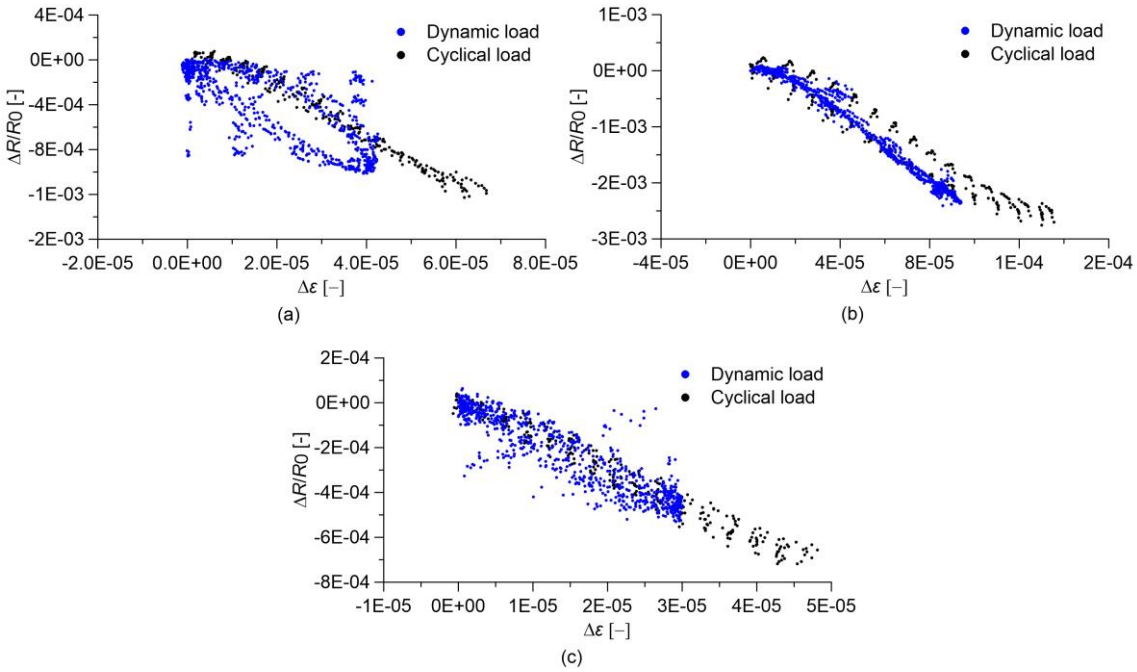

Figure 10. Relative change in electrical resistance versus applied strain of nanocomposite paste specimens. In the plots, R_0 is the electrical resistance value with a preload of 0.5 kN. Comparison between results obtained under dynamic compression loads and those obtained under cyclic compression loads: (**a**) Paste with 0.00% of MWCNTs; (**b**) Paste with 0.50% of MWCNTs; (**c**) Paste with 1.50% of MWCNTs.

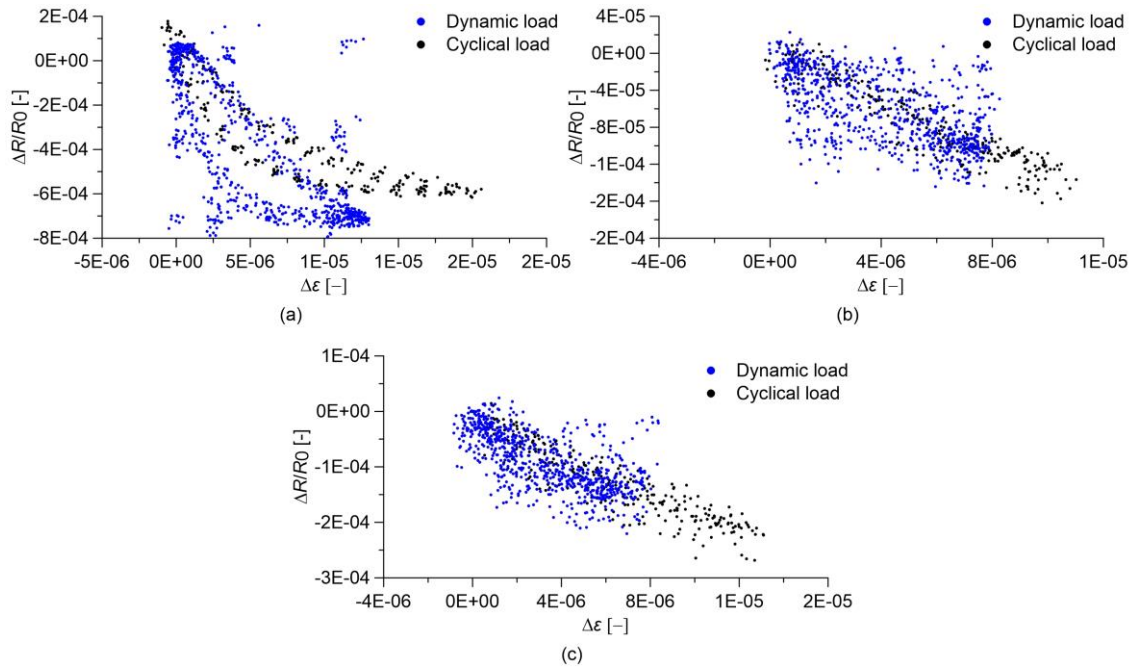

Figure 11. Relative change in electrical resistance versus applied strain of nanocomposite concrete specimens. In the plots, R_0 is the electrical resistance value with a preload of 0.5 kN. Comparison between results obtained under dynamic compression loads and those obtained under cyclic compression loads: (**a**) Concrete with 0.00% of MWCNTs; (**b**) Concrete with 0.50% of MWCNTs; (**c**) Concrete with 1.00% of MWCNTs.

Figures 8 and 9 report the time histories of the relative change in electrical resistance, $\Delta R/R_0$, and of the applied strain, $\Delta\varepsilon$, for cement paste and concrete specimens, considering the MWCNTs contents corresponding to the optimal gauge factor values. The presented results show that cement paste sensors exhibit a better signal quality in comparison to concrete sensors. Among cement paste ones, only the sensor containing 1.5% MWCNTs exhibits some signal distortions. It can be hypothesized that signal quality is highly affected by the quality of MWCNTs dispersion, which is less homogenous in concrete in comparison to cement paste due to the presence of the aggregates and also among paste sensors in the case of the specimen with a MWCNTs content of 1.5%, as already commented above.

3.4 Slow and fast varying response of the sensors

Another aspect potentially affecting the strain sensing behavior of cement-based nanocomposite sensors is represented by strain velocity effects. To better understand this aspect, Figures 10 and 11 show comparisons between the responses of the cement paste and concrete sensors under slowly varying cyclic and dynamic compressive loads. These results show that the plain materials, beside behaving nonlinearly, also exhibit an important hysteretic behavior under dynamic loads indicating a strong dependence of their electrical response under varying strain velocity. An increase in MWCNTs content has the effect of highly reducing such a hysteretic response.

3.5 Response of the sensors subjected to destructive tests

Figures 12 and 13 show stress and relative change in electrical resistance versus axial strain obtained from destructive compression tests carried out on cement paste and concrete specimens, respectively. In order to avoid possible measurement errors in estimating small axial strain values using data outputted by LVDTs displacement sensors installed in the testing machine, strain values in *x*-axes of Figures 12 and 13 are normalized by the strain at peak stress, denoted as ε_P. In both figures, plain samples are compared to the nanocomposite ones with the optimal gauge factor, corresponding to 0.5% and 1.0% of MWCNTs content for cement paste and concrete, respectively.

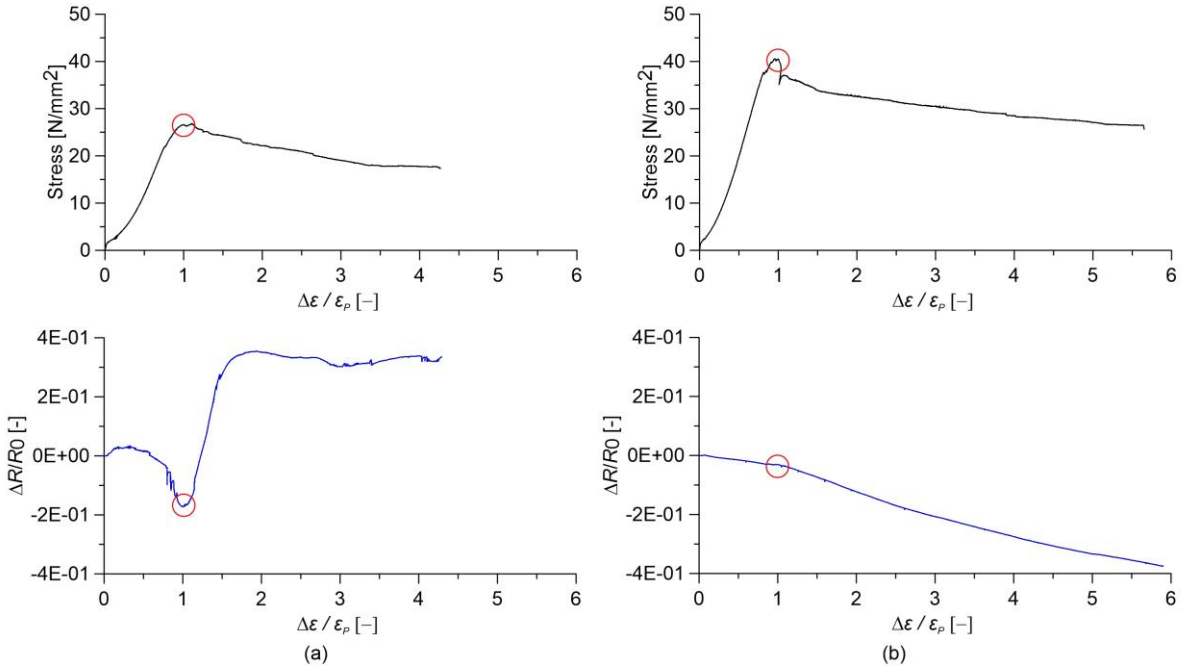

Figure 12. Comparison between stress and relative change in electrical resistance versus relative applied strain for paste specimens obtained from axial destructive tests (the circle indicates the peak stress point). (**a**) Paste with 0.00% of MWCNTs; (**b**) Paste with 0.50% of MWCNTs.

Preprints (www.preprints.org) | NOT PEER-REVIEWED | Posted: 7 February 2018 doi:10.20944/preprints201802.0063.v1

Peer-reviewed version available at Sensors 2018, 18, 831; doi:10.3390/s18030831

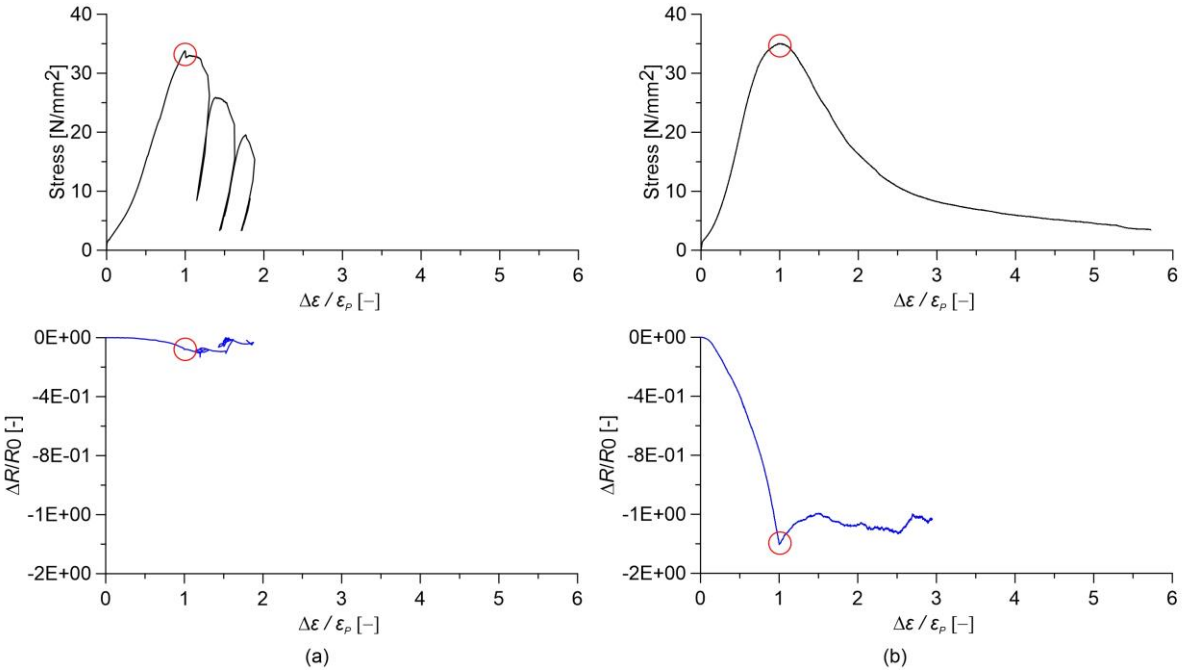

Figure 13. Comparison between stress and relative change in electrical resistance versus relative applied strain for concrete specimens obtained from destructive tests (the circle indicates the peak stress point). (**a**) Concrete with 0.00% of MWCNTs; (**b**) Concrete with 1.00% of MWCNTs.

Plain cement paste exhibits highly non-linear variation in relative change in electrical resistance with applied strain. In particular, when strain reaches ε_P, a sudden increase in the electrical resistance of the material is observed due to the formation of compression cracks (Figure 12a). Afterwards, any sensing function is lost. On the other hand, cement paste doped with 0.5% of MWCNTs exhibits a linear strain-sensing behavior, keeping the sensing capability up to the ultimate strain. However, a slight change in the gauge factor is noted at peak stress (Figure 12b). Strain sensitivity is essentially lacking in the case of plain concrete specimens (Figure 13a), while the addition of nanotubes results in a high variation in relative change in electrical resistance with strain, though slightly non-linear. Differently from the case of cement paste, the sensing function is lost after reaching the maximum axial stress (Figure 13b). Note that the addition of MWCNTs is seen to increase the axial compressive strength of cement paste, as well as the ratio between ultimate axial strain of concrete and corresponding ε_P, therefore increasing its ductility.

4. Discussion

This paper has investigated the electrical properties and the strain sensitivity of two different cementitious materials with increasing complexity of internal structure, namely Portland cement paste and concrete, and doped with various contents of MWCNTs.

The electrical tests, conducted with a 4-probe DC measurement methods, resulted in the identification of percolation thresholds between 1.0 and 1.5% with respect to the mass of the cement. Cementitious sensors were subjected to electromechanical tests in order to investigate their strain-sensing capability.

Test results highlighted that both plain and nanocomposite cement-based materials exhibit strain sensing capabilities, whereby their relative change in electrical resistivity is affected by the applied strain. Plain cement paste and plain concrete, however, exhibit a significantly non-linear and hysteretic response. The addition of carbon nanotubes regularizes such a strain-sensing response, making it linear and reversible, up to a volume fraction of carbon nanotubes that is slightly below the percolation

threshold. At percolation, the response becomes slightly non-linear, while the linearity seems to recover for higher nanotube content.

When applying slowly varying cyclic, as well as dynamic compression harmonic loads of increasing frequency, cement paste sensors exhibit a better quality of signals compared to concrete sensors in terms of signal-to-noise ratio. Cement paste sensors exhibiting the most linear behavior under slow cyclic loads also exhibit the least hysteretic response under dynamic load. A similar trend for concrete sensors is not so apparent.

Destructive compression tests in controlled displacement conditions were performed in order to investigate the strain sensing capability under large compressive strain up to the ultimate conditions of the materials. The results have highlighted the better strain sensing capability of the composite materials in comparison to plain ones. Cement paste doped with nanotubes held such a strain-sensing capability even after the peak compressive stress. An improvement in mechanical properties due to the introduction of carbon nanotubes is also evidenced for both paste and concrete specimens.

5. Conclusions

Results of the present research have confirmed that cement-based sensors doped with carbon nanotubes are promising for civil engineering applications, but the amount of nanotubes, the quality of their dispersion and the presence of aggregates are key factors that can highly affect their strain sensing behavior. Overall, it is concluded that nanocomposite cement paste sensors are more appropriate than concrete ones for strain sensing in both static and dynamic conditions, because concrete samples exhibited a higher level of noise conceivably due to a less homogeneous nanotube dispersion. The same result has been obtained in destructive tests where nanocomposite cement paste has been found capable to hold the strain-sensing capabilities even after reaching the maximum compressive stress. Moreover, using cement paste sensors, a smaller level of carbon nanotubes, in this research identified around 0.5% with respect to the mass of cement, can be sufficient to achieve a good and linear strain sensitivity.

Acknowledgments: The support of the Italian Ministry of Education, University and Research (MIUR) through the funded Project of Relevant National Interest "SMART-BRICK: Novel strain-sensing nano-composite clay brick enabling self-monitoring masonry structures" is gratefully acknowledged. This work is also partly supported by the National Science Foundation Grant No. 1069283, which supports the activities of the Integrative Graduate Education and Research Traineeship (IGERT) in Wind Energy Science, Engineering and Policy (WESEP) at Iowa State University. Their support is gratefully acknowledged.

Authors Contributions: Andrea Meoni took care of the write-up and of data analysis; Antonella D'Alessandro led the experiments; Austin Downey established the protocol for electrical measurements; Enrique García-Macías developed theoretical micromechanics models interpreting the results; Marco Rallini and Luigi Torre led material processing and analysis; Luigi Materazzi, Simon Laflamme, Rafael Castro-Triguero and Filippo Ubertini provided scientific guidance on SHM; Simon Laflamme and Filippo Ubertini proof-read the manuscript.

Conflicts of Interest: The authors declare no conflict of interest.

References

1. Shah, S.P.; Konsta-Gdoutos, M.S.; Metexa, Z.S.; Mondal, P. Nanoscale Modification of Cementitious Materials. In *Nanotechnology in Construction 3*; Bittnar, Z. et al; Springer, Berlin, Heidelberg, 2009; pp. 125-130, 978-3-642-00979-2.
2. Mondal, P.; Shah, S.P.; Marks, L.D. Nanoscale characterization of cementitious materials; *ACI Mat. J.* **2008**, 105, pp. 174-179.
3. Brownjohn, J.M.W. Structural health monitoring of civil infrastructure. *Philos T. R. Soc.* **2007**, A 365(1851), pp. 589-622, DOI: 10.1098/rsta.2006.1925.
4. Magalhaes, F.; Cunha, A.; Caetano, E. Vibration based structural health monitoring of an arch bridge: From automated OMA to damage detection. *Mech. Syst. Sig. Proc.* **2012**, 28, pp. 212-228.

5. Laflamme, S.; Ubertini, F.; Saleem, H.; D'Alessandro, A.; Downey, A.; Ceylan, H.; Materazzi, A.L. Dynamic Characterization of a Soft Elastomeric Capacitor for Structural Health Monitoring. *J. Struct. Eng. in press available online*, DOI:10.1061/(ASCE)ST.1943-541X.0001151, 04014186 (2014).
6. Han, B.; Wang, Y.; Dong, S.; Zhang, L.; Ding, S.; Yu, X.; Ou, J. Smart concretes and structures: A review. *J. Intell. Mater. Syst. Struct.* **2005,** 26 (11), pp. 1303-1345.
7. Muto, N.; Yanagida, H.; Nakatsuji, T.; Sugita, M.; Ohtsuka, Y.; Arai, Y. Design of intelligent materials with self-diagnosing function for preventing fatal fracture. *Smart Mater. Struct.* **1992,** vol. 1, no. 4, pp. 324-329.
8. Chen, P-W.; Chung, D.D.L. Carbon fiber reinforced Concrete for smart structures capable of non-destructive flaw detection. *Smart Mater. Struct* **1993**, vol. 2, pp. 22-30.
9. Ji, T.; Zhang, X.; Li, W. Enhanced thermoelectric effect of cement composite by addition of metallic oxide nanopowders for energy harvesting in buildings. *Construction and Building Materials* **2016**, 115, pp. 576–581.
10. Yang, Y.; Li, M.; Wu, Y.; Choo, T.E.S.G.; Ding, J.; Zong, B.; Yang, Z.; Xue, J. Nanoscaled self-alignment of Fe3O4 nanodiscs in ultrathin rGO films with engineered conductivity for electromagnetic interference shielding. *Nanoscale* **2016**, 8(35), pp. 15989-15998.
11. Bragaru, A.; Kusko, M.; Vasile, E.; Simion, M.; Danila, M.; Ignat, T.; Mihalache, I.; Pascu, R.; Craciunoiu, F. Analytical characterization of engineered ZnO nanoparticles relevant for hazard assessment. *Journal of Nanoparticle Research* **2013**, 15:1352, DOI 10.1007/s11051-012-1352-0.
12. Xiong, X.; Busnaina, A. Direct assembly of nanoparticles for large-scale fabrication of nanodevices and structures. *Journal of Nanoparticle Research* **2008**, 10(6), pp 947–954.
13. García, A.; Schlangen, E.; van de Ven, M.; Liu, Q. Electrical conductivity of asphalt mortar containing conductive fibers and fillers. *Construction and Building Materials* **2009**, 23(10), pp. 3175-3181.
14. Li, G.Y.; Wang, P.M.; Zhao, X. Pressure-sensitive properties and microstructure of carbon nanotube reinforced cement composites. *Cem. Concr. Comp.* **2007**, 29, pp. 377-382.
15. Rhee, I.; Lee, J.S.; Kim, Y.A.; Kim, J.H. Electrically conductive cement mortar: Incorporating rice husk-derived high-surface-area graphene. *Construction and Building Materials* **2016**, 125, pp. 632–642.
16. Chuah, S.; Pan, Z.; Sanjayan, J.G.; Wang, C.M.; Duan, W.H. Nano reinforced cement and concrete composites and new perspective from graphene oxide. *Construction and Building Materials* **2014**, 73, pp. 113–124.
17. Tamimi, A.; Hassan, N.M.; Fattah, K; Talachi, A. Performance of cementitious materials produced by incorporating surface treated multiwall carbon nanotubes and silica fume. *Construction and Building Materials* **2016**, 114, pp. 934–945.
18. Siddique, R.; Mehta, Ar. Effect of carbon nanotubes on properties of cement mortars. *Construction and Building Materials* **2014**, 50, pp. 116–129.
19. Morsy, M.S.; Alsayed, S.H.; Aqel, M. Hybrid effect of carbon nanotube and nano-clay on physico-mechanical properties of cement mortar. *Construction and Building Materials* **2011**, 25, pp. 145–149.
20. Camacho-Ballesta, C.; Zornoza, E.; Garcés, P. Performance of cement-based sensors with CNT for strain sensing. *Advances in Cement Research* **2016**, 28 (4), pp. 274-284.
21. Ubertini, F.; Laflamme, S.; D'Alessandro, A. Smart cement paste with carbon nanotubes. In: *Innovative Developments of Advanced Multifunctional Nanocomposites in Civil and Structural Engineering;* K.J. Loh and S. Nagarajaiah; Woodhead Publishing, 2016, pp. 97-120.
22. Shah, S.P.; Konsta-Gdoutos, M.S.; Metexa, Z.S.; Mondal, P. Nanoscale Modification of Cementitious Materials. In: *Nanotechnology in Construction 3*; Bittnar, Z. et al; Springer, Berlin, 2009, pp. 125-130.
23. D'Alessandro, A.; Fabiani, C.; Pisello, A.L.; Ubertini, F.; Materazzi, A.L.; Cotana, F. Innovative concretes for low carbon constructions: a review. *Int. J. Low-Carbon Tech. in press (2016).*
24. Liu, M.; Frangopol, D.M.; Kwon, K. Fatigue reliability assessment of retrofitted steel bridges integrating monitoring data. *Struct. Saf.* **2010**, 32(1), pp. 77-89.
25. Yining, D.; Chen, Z.; Han, Z.; Zhang, Y.; Pacheco-Torgal, F. Nano-carbon black and carbon fiber as conductive materials for the diagnosing of the damage of concrete beam. *Construction and Building Materials* **2013**, 43, pp. 233–241.
26. Mosquera, V.; Smyth, A.W.; Betti, R. Rapid Evaluation and Damage Assessment of Instrumented Highway Bridges. *Earthq. Eng. Struc.* **2012**, 41(4), pp. 755-774.
27. Han, B.; Yu, X.; Kwon, E. A self-sensing carbon nanotube/cement for traffic monitoring. *Nanotechnology* **2009**, 20, DOI: 10.1088/0957-4484/20/44/445501.
28. Han, B.; Yu, X.; Ou, J. *Self-sensing concrete in smart structures*; Butterworth-Heinemann, Elsevier, 2014.

29. Zhou, X.; Xi, L.; Lee, J. Reliability-centered predictive maintenance scheduling for a continuously monitored system subject to degradation. *Rel. Eng. Syst. Saf.* **2007**, 92(4), pp. 530-534.
30. Spencer Jr, B.F.; Ruiz-Sandoval, M.E.; Kurata, N. Smart sensing technology: opportunities and challenges. *Struct. Control Health Monit.* 2004, 11, pp. 349-368.
31. Yu, X.; Kwon, E. A carbon nanotube/cement composite with piezoresistive properties. *Smart Mater. Struct.* **2009**, 18, 5pp.
32. Hou, T.C.; Lynch, J.P. Conductivity-based strain monitoring and damage characterization of fiber reinforced cementitious structural components. Proc. SPIE, *The International Society for Optical Engineering* **2005,** 5765 (PART 1) 44, pp. 419-429.
33. Luo, J.; Duan, Z.; Zhao, T.; Li, Q. Hybrid effect of carbon fiber on piezoresistivity of carbon nanotube cement-based composite. *Adv. Mat. Res.* **2011,** 143-144, pp. 639-643.
34. Konsta-Gdoutos, M.S.; Aza, C.A. Self sensing carbon nanotube (CNT) and nanofiber (CNF) cementitious composites for real time damage assessment in smart structures. *Cem. Conc. Comp.* **2014**, 53, pp. 110-128.
35. Zhu, Z.H. Piezoresistive strain sensors based on carbon nanotube networks: Contemporary approaches related to electrical conductivity. *IEEE Nanotechnology Magazine* **2015**, 9(2), pp. 11-23.
36. Li, H.; Xiao, H; Ou, J. A study on mechanical and pressure-sensitive properties of cement mortar with nanophase materials. *Cem. Concr. Res.* **2003**, 34, pp. 435-438.
37. Wen, S.; Chung, D.D.L. Model of piezoresistivity in carbon fiber cement. *Cem. Concr. Res.* **2006**, 36, pp. 1879-1885.
38. Galao, O.; Baeza F.J.; Zornoza, E.; Garcés, P. Strain and damage sensing properties on multifunctional cement composites with CNF admixture. *Cem. Concr. Comp.* **2014**, 46, pp. 90-98.
39. D'Alessandro, A.; Ubertini, F.; Materazzi, A.L.; Porfiri, M.; Laflamme, S. Electromechanical Modelling of New Nanocomposite Carbon Cement-based Sensors for Structural Health Monitoring. *Struct. Heal. Monit., in press available online, doi:10.1177/1475921714560071 (2014).*
40. Azhari, F.; Banthia, N. Cement-based sensors with carbon fibers and carbon nanotubes for piezoresistive sensing. *Cem. Concr. Comp.* **2012**, 34, pp. 866-73.
41. Li, H.; Xiao, H.; Ou, J. Effect of compressive strain on electrical resistivity of carbon black-filled cement-based composites. *Cem. Concr. Comp.* **2006**, 28, pp. 824-828.
42. Wen, S.; Chung, D.D.L. Partial Replacement of Carbon Fiber by Carbon Black in Multifunctional Cement-Matrix Composites. *Carbon* **2007**, 45(3), pp. 505-513.
43. Chuah, S.; Pan, Z.; Sanjayan, J.G.; Wang, C.M.; Duan, W.H. Nano reinforced cement and concrete composites and new perspective from graphene oxide. *Constr. Build. Mater.* **2014**, 73, pp. 113-124.
44. Mondal, P.; Shah, S.P.; Marks, L.D. Nanoscale characterization of cementitious materials. *ACI Mat. J.* **2008**, 105, pp. 174-179.
45. Han, B.; Yu, X.; Ou, J. Multifunctional and smart nanotube reinforced cement-based materials. In *Nanotechnology in Civil Infrastructure*; A Paradigm shift. Gipalakrishnan K., Birgisson B., Taylor P., Attoh-Okine N. Editors – Springer (2011) 1-48.
46. Makar, J.; Beaudoin, J. Carbon nanotubes and their application in the construction industry. In: *Proceedings of the 1st international symposium on nanotechnology in construction* (NICOM 2003); Bartos, P., et al., eds., 331–341.
47. Chen, S.J.; Collins, F.G.; Macleod, A.J.N.; Pan, Z.; Duan, W.H.; Wang, C.M. Review Paper. Carbon nanotube-cement composites: A retrospect. *The IES Journal Part A: Civil and Structural Engineering* **2011**, 4(4), pp. 254-265.
48. Li, B.; Li, L.; Wang, B.; Li, C.Y. Alternating patterns on single-walled carbon nanotubes. *Nature Nanotechnology* **2009**, 4, pp. 358–362.
49. Materazzi, A.L.; Ubertini, F.; D'Alessandro, A. Carbon nanotube cement-based transducers for dynamic sensing of strain. *Cem. Conc. Comp.* **2013**, 37, pp. 2-11.
50. Lourie, O.; Wagner, D.E. Buckling and collapse of embedded carbon nanotube. *Phys. rev. Lett.* **1998**, 81(8), pp. 1638-1641.
51. Loh, K.J.; Gonzalez, J. Cementitious Composites Engineered with Embedded Carbon Nanotube Thin Films for Enhanced Sensing Performance. *Journal of Physics: conference Series*, **2015**, 628, 012042.
52. Abu Al-Rub, R.K.; Ashour, A.I.; Tyson, B.M. On the aspect ratio effect of multi-walled carbon nanotube reinforcements on the mechanical properties of cementitious nanocomposites. *Constr. Build. Mater.* **2012**, 35, pp. 647-655.

53. Hilding, J.; Grulke, E.A.; Zhang, Z.G.; Lockwood, F. Dispersion of carbon nanotubes in liquids. *Journal of Dispersion Science and Technology* **2003**, 24, pp. 1–41.
54. D'Alessandro, A.; Rallini, M.; Ubertini, F.; et al. Investigations on scalable fabrication procedures for self-sensing carbon nanotube cement-matrix composites for SHM applications. *Cem. Concr. Comp.* **2016**, 65, pp. 200-213.
55. Han, B.; Ding, S.; Yu, X. Intrinsic self-sensing concrete and structures: A review. *Measurements* **2015**, 59, pp. 110-128.
56. Ubertini, F.; Laflamme, S.; Ceylan, H.; Materazzi, A.L.; Cerni, G.; Saleem, H.; D'Alessandro, A.; Corradini, A. Novel Nanocomposite Technologies for Dynamic Monitoring of Structures: a Comparison between Cement-Based Embeddable and Soft Elastomeric Surface Sensors. *Smart Mater. Struct* **2014**, 23(4), 12pp.
57. Cao, J.; Chung, D.D.L. Electric polarization and depolarization in cement-based materials, studied by apparent electrical resistance measurement. *Cem. Concr. Res.* **2004**, 34, pp. 481-485.
58. Wen, S.; Chung, D.D.L. Damage monitoring of cement paste by electrical resistance measurement. *Cem. Concr. Res.* **2000**, 30, pp. 1979-1982.
59. Han, B.; Ou, J. Embedded piezoresistive cement-based stress/strain sensors. *Sensor Actuat. A - Phys.* **2007**, 138, pp. 294-298.
60. Xie, P.; Gu, P.; Beaudoin, J.J. Electrical percolation phenomena in cement composites containing conductive fibers. *J. Mater. Sci.* **1996**, 31, pp. 4093-4097.
61. Wen, S.; Chung, D.D.L. Double percolation in the electrical conduction in carbon fiber reinforced cement-based materials. *Carbon* **2007**, 45, pp. 263-267.
62. Wansom, S.; Kidner, N.J.; Woo, L.Y.; Mason, T.O. AC-impedance response of multi-walled carbon nanotube/cement composites. *Cem. Concr. Comp.* **2006**, 28, pp. 509-519.
63. García-Macías, E.; D'Alessandro, A.; Castro-Triguero, R.; Pérez-Mira, D.; Ubertini, F. Micromechanics modeling of the electrical conductivity of carbon nanotube cement-matrix composites. *Composites Part B: Engineering* **2017**, 108, pp. 451-469.
64. Nadiv, R.; Vasilyev, G.; Shtein, M.; Peled, A.; Zussman, E.; Regev, O. The multiple roles of a dispersant in nanocomposite systems. *Composites Science and Technology* **2016**, 133(14), pp. 192-199.
65. Materazzi, A.L.; Ubertini, F.; D'Alessandro, A. Carbon nanotube cement-based transducers for dynamic sensing of strain. *Cem Conc Comp* **2013**, 37, pp. 2-11.
66. Ubertini, F.; Materazzi, A.L.; D'Alessandro, A.; Laflamme, S. Natural frequencies identification of a reinforced concrete beam using carbon nanotube cement-based sensors. *Eng. Struct.* **2014**, 60, pp. 265-275.
67. Page McAndrew, T.; Laurent, P.; Havel, M.; Roger, C. Arkema graphistrength® multi-walled carbon nanotubes, Technical Proceedings of the 2008 NSTI Nanotechnology Conference and Trade Show, NSTI-Nanotech. *Nanotechnology* **2008**, 1, pp. 47-50.